Aeroacoustic Study of a High-Fidelity Aircraft Model: Part 2—Unsteady Surface Pressures

Mehdi R. Khorrami[1] and Dan H. Neuhart[2]
NASA Langley Research Center, Hampton, Virginia, 23681

In this paper, we present unsteady surface pressure measurements for an 18%-scale, semi-span Gulfstream aircraft model. This high-fidelity model is being used to perform detailed studies of airframe noise associated with main landing gear, flap components, and gear–flap interaction noise, as well as to evaluate novel noise reduction concepts. The aerodynamic segment of the tests, conducted in the NASA Langley Research Center 14- by 22-Foot Subsonic Tunnel, was completed in November 2010. To discern the characteristics of the surface pressure fluctuations in the vicinity of the prominent noise sources, unsteady sensors were installed on the inboard and outboard flap edges, and on the main gear wheels, struts, and door. Various configurations were tested, including flap deflections of 0º, 20º, and 39º, with and without the main landing gear. The majority of unsteady surface pressure measurements were acquired for the nominal landing configuration where the main gear was deployed and the flap was deflected 39º. To assess the Mach number variation of the surface pressure amplitudes, measurements were obtained at Mach numbers of 0.16, 0.20, and 0.24. Comparison of the unsteady surface pressures with the main gear on and off shows significant interaction between the gear wake and the inboard flap edge, resulting in higher amplitude fluctuations when the gear is present.

Nomenclature

AOA	=	angle-of-attack
C_L	=	lift coefficient
Cp'_{rms}	=	unsteady RMS pressure coefficient
Cp	=	pressure coefficient
C	=	local chord
GAC	=	Gulfstream Aerospace Corporation
Hz	=	Hertz, cycles per second
M	=	Mach number
PSD	=	power spectral density in psi^2/Hz
psf, psi	=	pounds per square foot, pounds per square inch
Q	=	wind tunnel dynamic pressure in psf
Re	=	Reynolds number
RMS	=	root mean square
t_i	=	flap maximum thickness at inboard edge
t_o	=	flap maximum thickness at outboard edge
U	=	uncertainty in measured quantities
X	=	coordinate along chord

I. Introduction

A substantial reduction in the environmental effects of civil aviation operations near airports is a major goal of NASA. During approach-to-landing operations, the airframe component of aircraft noise is comparable to engine noise. Thus, if the total noise produced by modern civil transports is to be reduced significantly, airframe noise must be addressed. Acoustic measurements from both flight tests[1-6] and model-scale experiments[7-8] have identified the undercarriage system and high-lift devices, such as slats and flaps, as the prominent sources of airframe noise. Airframe noise reduction technologies that will maintain the aerodynamic efficiency of the airframe need to be

[1] Aerospace Engineer, Computational AeroSciences Branch, Associate Fellow AIAA
[2] Aerospace Engineer, Flow Physics and Control Branch

developed and evaluated. An essential element for the successful development of appropriate noise reduction technologies is the availability of a high-fidelity, large-scale airframe model to facilitate the assessment of candidate concepts under relevant flight conditions.

As part of the NASA-Gulfstream partnership on airframe noise research, a carefully planned series of flight tests and model scale experiments are being conducted with a Gulfstream aircraft as the baseline configuration. The joint effort began with an acoustic flight test in 2006 where the prominent airframe noise sources associated with a Gulfstream aircraft were identified and documented.[8] The major noise sources are the flap side-edges, main landing gear, and nose landing gear. Gear–flap flow interaction was also recognized as a potential noise source. Because of the relative structural isolation of the nose landing gear, a decision was made to investigate that source independently from the other sources. The aeroacoustic studies of a Gulfstream nose landing gear have been documented in previous papers.[9, 10] An 18% scale, semi-span replica of a Gulfstream aircraft has been designed and fabricated specifically to conduct airframe noise studies and evaluate noise reduction concepts for mitigating landing gear, flap, and gear–flap interaction noise.

Aeroacoustic testing of the 18% scale semi-span model is being performed as a series of carefully planned entries in the NASA Langley Research Center (LaRC) 14- by 22-Foot Subsonic Tunnel (14x22). The initial entry, completed in November 2010, focused on acquiring global forces (lift and drag) and measurements of steady and unsteady surface pressures. The second 14x22 tunnel entry will be executed in two segments. The first segment will be dedicated to simultaneous acoustic and surface pressure measurements, while the second segment will be devoted to performing off-surface flow measurements for the nominal aircraft landing configuration.

A full account of the 18% scale semi-span model lift, drag and steady surface pressures is given in a companion paper by Khorrami et al.[11] The present paper provides a detailed description of the measured fluctuating surface pressures in regions pertinent to the prominent airframe noise sources.

II. Model Description

The model is an 18% scale semi-span high-fidelity reproduction of a Gulfstream aircraft (see Fig. 1). It was designed, fabricated, instrumented, and integrated at NASA LaRC based on a set of geometry files provided by the Gulfstream Aerospace Corporation (GAC). The model geometry consists of a fuselage, wing, flap, flow-through nacelle, pylon, and main landing gear. A full description of this model, including the reasons for choosing the semi-span configuration and 18% as the model scale, is provided in Ref. 11. Also discussed in Ref. 11 is the model instrumentation as it relates to the distribution of steady pressure ports on various components. In the present paper, only those details that are pertinent to the unsteady pressure measurements will be provided.

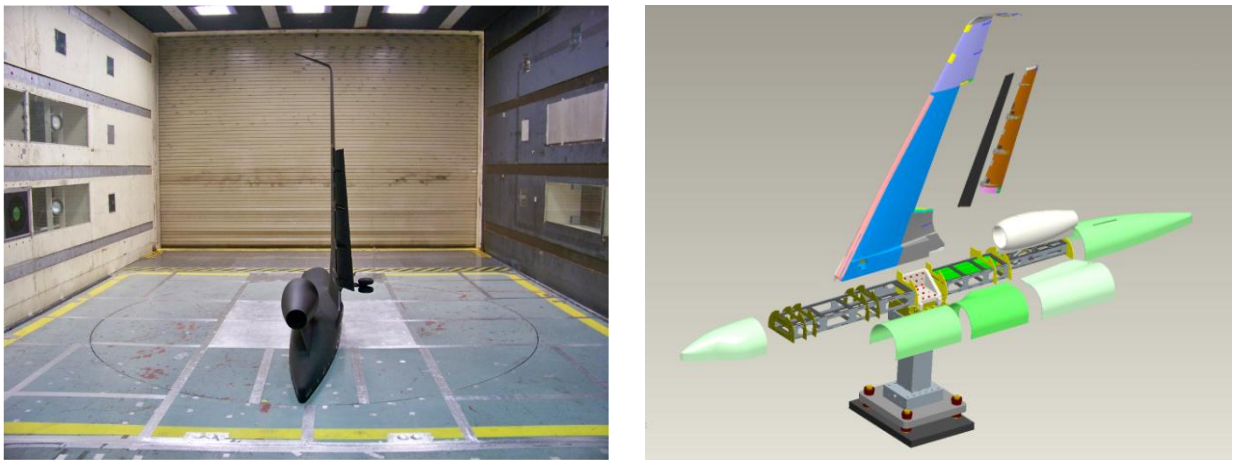

a) Installed in NASA LaRC 14x22 tunnel b) Exploded view of model

Figure 1. 18% scale semi-span model of a Gulfstream aircraft.

A. Model Instrumentation

To improve our understanding of the principles of airframe noise generation, and to help validate and advance computational simulation tools, extensive measurements of steady and unsteady, on-surface and off-surface flows, and the associated acoustic fields, must be acquired. Because of physical limitations on the amount of

instrumentation that can be installed in a particular component, the distribution of the unsteady pressure sensors was chosen to facilitate a detailed assessment of the complex flow features that generate noise. Accordingly, the prominent noise sources, such as the flap inboard and outboard edges and the various components of the main landing gear were populated with pressure sensors. In total, 69 dynamic pressure transducers, 12 accelerometers, and 758 static pressure ports were installed on the model. An account of the static port distribution on various components is given in the companion paper by Khorrami et al.[11] A brief description of unsteady sensor placement is provided below.

The majority of the installed pressure sensors were Kulite® differential unsteady pressure transducers (model LQ-12A-062-2D) having a 0.040" (1.0 mm) opening diameter. The flush mounted differential transducers provide a dynamic range of -2.0 psi (-13.79 kPa) to 0.6 psi (4.14 kPa) and a frequency range of 0 to 16 kHz. These 57 differential sensors were calibrated in situ over the operating pressure range plus 2% (-2.04 to 0.612 psi) by applying the corresponding opposite-sign pressure to the reference side of the transducers. A highly-accurate reference pressure controller (Ruska) applied five test pressures over the range and then a linear fit was applied to the DC signal, to yield in-situ sensitivity coefficients. Typically, these coefficients were different than the "out-of-the-box" values by a few percentage points. To gain higher frequency resolution while sacrificing some sensitivity, Kulite® absolute transducers (model LQ-41-064-16A) having a 0.025" (0.6 mm) opening diameter were used in some locations. The absolute transducers provide a dynamic range of 0 psi (0 Pa) to 16 psi (110.3 kPa) at 25 kHz. For these sensors, their "out-of-the-box" sensitivity coefficients were used.

Of the 69 dynamic sensors, 40 were installed on the flap. To cover the regions of interest, the sensors were distributed in three distinct areas: along the mid-span section, subsequently referred to as the main body of the flap, and two narrow spanwise strips adjacent to the inboard and outboard edges. Figure 2 displays a top and bottom view of the entire 18% scale model flap, highlighting the locations of the sensors (from now on referred to as probes to be consistent with the ongoing computational effort) and their assigned identification numbers on the central part of the flap. The two streamwise broken lines near the inboard and outboard edges mark spanwise distances corresponding to one and two times the maximum flap thickness at those locations. To understand the extent and nature of flow separation, the majority of the probes on the upper surface were installed in a streamwise row corresponding to the flap mid-span position. Probes 21 and 17 were placed at the same chordwise position on the upper and lower surfaces, respectively, near the trailing edge. Measurements from these probes will provide insight on the surface pressure features associated with the turbulent boundary layers passing over the trailing edge at moderate and high flap deflection angles.

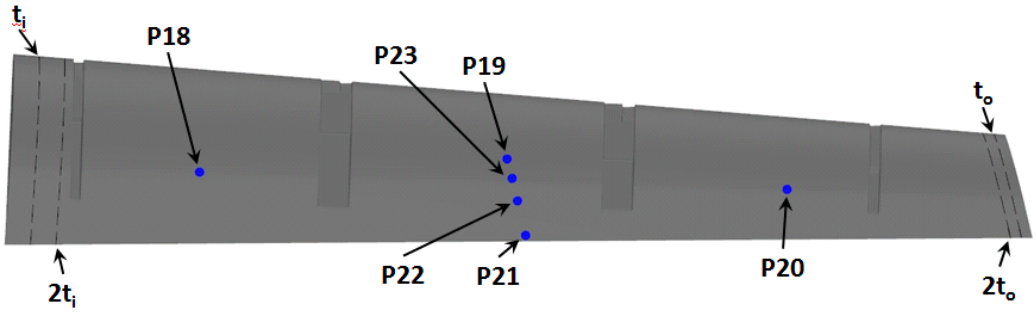

a) Top view

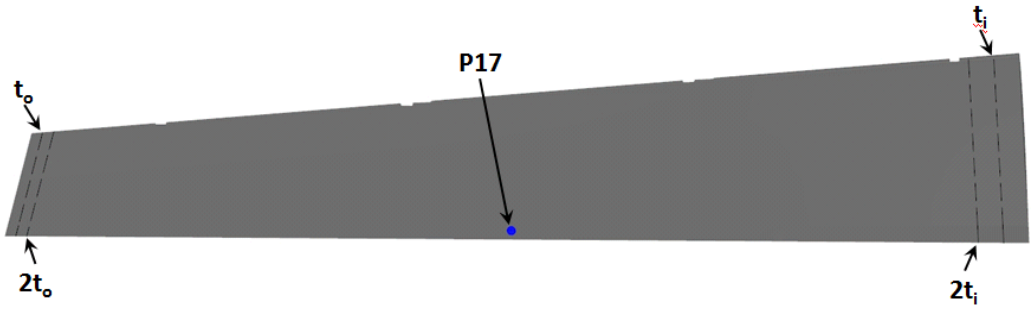

b) Bottom view

Figure 2. Locations and numbering of surface pressure probes on the main body of the flap.

To capture the effect of gear–flap flow interaction as well as the vortex roll-up process, the inboard flap edge was populated with the highest concentration of surface pressure probes. The spatial distribution of the probes in the strip adjacent to the inboard flap edge is shown in Fig. 3. Note that most of the probes have been placed within a spanwise strip that is barely wider than one local flap maximum thickness as shown by the chordwise broken lines. This placement was based on past experiences with flap side-edge vortices, where the vortex systems typically reside within a narrow region between one to two times the maximum flap thickness. Note that four probes have also been installed on the flap edge sidewall.

The red dots in Fig. 3 indicate non-functioning (dead) probes. Although extreme care was taken to ensure proper handling of the probes during their installation on the semi-span model, five of the probes, placed on various model components, failed during model transport and installation in the 14x22 tunnel. Unfortunately, the tight packaging of the model precludes replacing these probes without damaging existing probes.

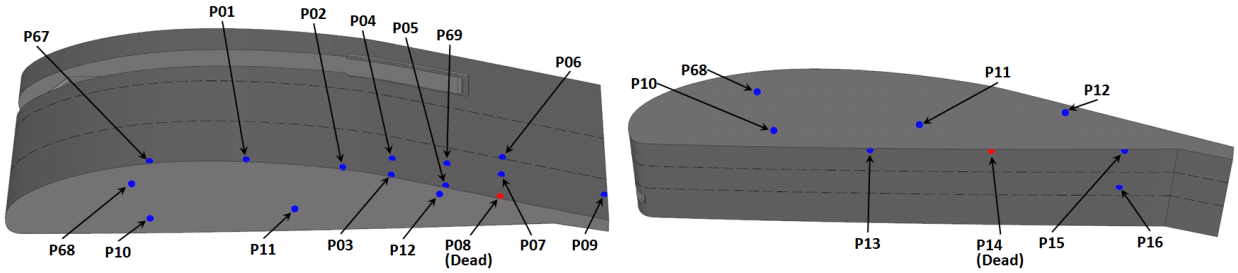

a) Top and side view. b) Bottom and side view.

Figure 3. Locations and numbering of probes installed at the flap inboard edge.

Probe locations for the flap outboard edge are shown in Fig. 4. Similarly to the inboard edge, most of the probes were placed within one or two times the local flap maximum thickness. Note that the flap side-edge has a cavity that nearly spans the entire chord length. In the actual aircraft, the function of this cavity is to house a bulb seal that prevents metal to metal contact during flap retraction. To document whether the cavity acoustic modes get excited at high flap deflections, two probes (26 and 27) were installed inside the cavity.

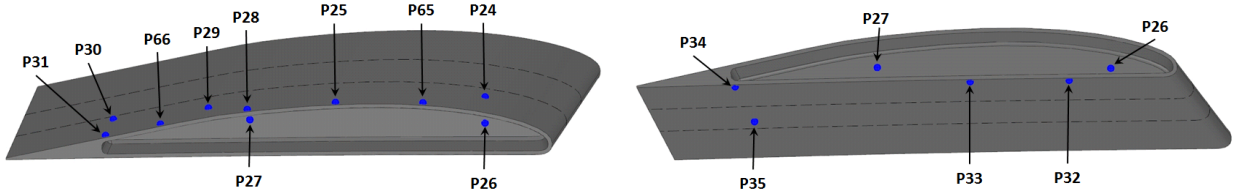

a) Top and side view. b) Bottom and side view.

Figure 4. Locations and numbering of probes installed at the flap outboard edge.

In total, 29 probes were installed on the main gear components. Side and rear views of the main landing gear are displayed in Fig. 5, identifying the major subcomponents housing the unsteady surface probes. For reference, the wheel on the same side as the gear door is identified as the "outer" wheel (closest to the wing tip) and the other as the "inner" wheel (closest to the fuselage). The locations of the probes on the main gear were chosen based on the insights gained from the earlier isolated nose gear aeroacoustic studies.[9,10] Probes were installed on the wheels, door, main post (front strut) and shock (rear) strut. Probe distributions on the various gear components are shown in Figs. 6 through 8. Three of the probes on the gear were discovered to be dead (one on each wheel and one on the door). The probes on each wheel are arranged in one transverse row positioned at an angle of 130º, as shown in Fig. 5a. The wheels are designed to be rotated ±30º in 10º increments to increase the resolution of the surface pressure measurements on the tires.

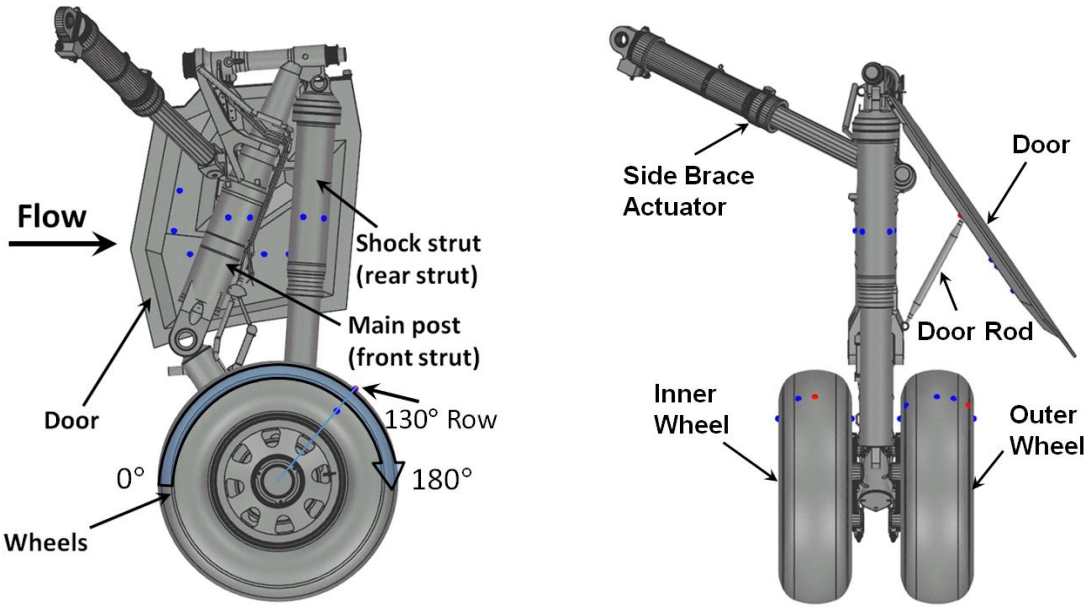

a) Side view. b) Rear view.

Figure 5. Side and rear views of the main landing gear highlighting major components.

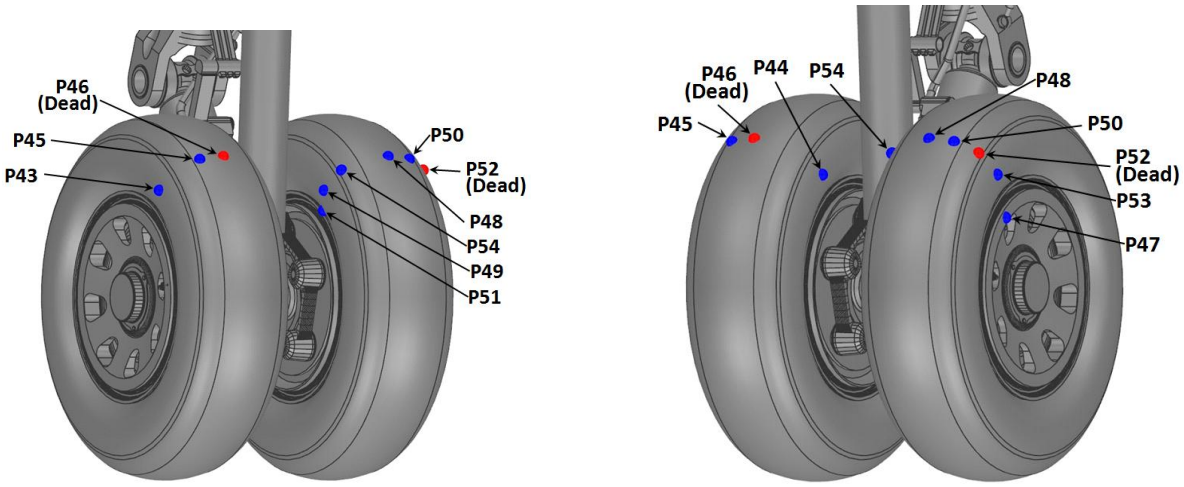

a) Interior (fuselage) view. b) Exterior (wing-tip) view.

Figure 6. Interior and exterior views of the wheels showing the locations of the installed probes.

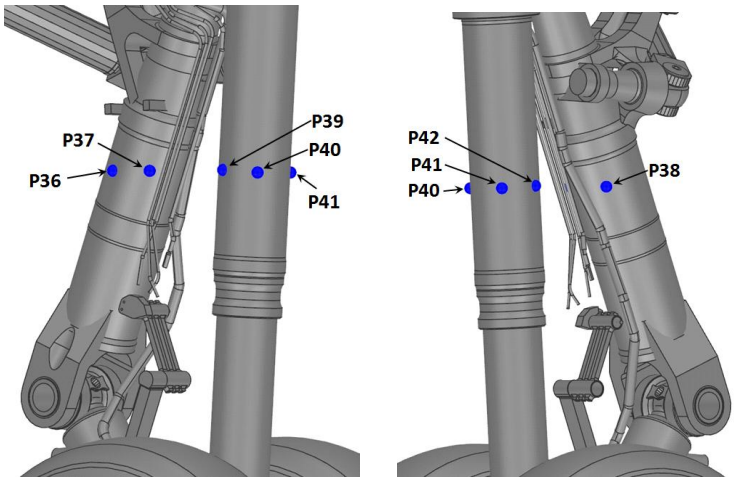

a) Interior (fuselage) view b) Exterior (wing-tip) view

Figure 7. Interior and exterior views of main post and shock strut.

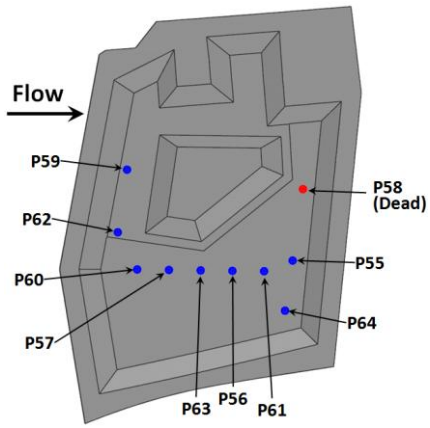

Figure 8. Door interior side

B. Unsteady Pressure Measurements

Simultaneous recording of the pressure signal from all 64 functioning Kulite® probes was accomplished. The unsteady pressure data were acquired at a sample rate of 51.2 kHz, yielding a bandwidth of 20 kHz. The data were analyzed to obtain the power spectral density (PSD) by using 100 blocks of 8,192 points. The resulting frequency resolution of the PSD was 6.25 Hz. A Hanning window was applied to each block. The PSD data were integrated to provide a mean square value of the fluctuating pressure for each probe at each condition. Taking the square root of each mean square value, giving the RMS (root mean square) pressure fluctuation, and dividing by the freestream dynamic pressure yielded the unsteady RMS pressure coefficient (Cp'_{rms}).

The approach outlined in Ref. 12 was used to perform the uncertainty analysis for both measured and calculated (PSD, Cp'_{rms} and coherence) quantities. Uncertainties in these calculated quantities were estimated to be the following: $U_{PSD}/PSD = 0.12$ (12%), $U_{Cp'rms}/Cp'_{rms} = 0.06$ (6%), and for coherence, the uncertainty varies as shown in Table 1.

Table 1. Uncertainty associated with computed coherence

Coherence	U_{coh}
1	0
0.75	0.04
0.5	0.1
0.25	0.21
0	infinite

III. Results

The first entry into the LaRC 14x22 tunnel was completed during November 2010. This test was devoted entirely to the detailed mapping of the aerodynamic characteristics of the model. Configurations of 39º, 20º, and 0º flap deflections, with the main landing gear on and off, were tested at Mach numbers of 0.16, 0.20, and 0.24. Additionally, for each flap deflection, the model was tested with the 14x22 tunnel in both the closed-wall and open-wall (jet) modes.[13] Because of the specific interest in airframe noise during landing operations, the 39º flap setting was the most heavily tested configuration of the experiment. Therefore, results for this baseline setting at Mach 0.20 with the tunnel walls closed are the focus of the present paper.

A. Test Conditions

Most of the data were taken for a nominal Mach number of 0.20. At this Mach number, the tunnel dynamic pressure, Q, and the freestream speed are 58 psf (2.77 kPa) and 223 ft/sec (68 m/sec), respectively. The corresponding Reynolds number is 1.33 million per foot (4.40 million per meter) resulting in a value of 3.40 million based on the 18% model mean aerodynamic chord of 30.8" (0.782 m). Based on a previous study,[14] the freestream turbulence level in the 14x22 tunnel (in the closed-wall configuration) typically ranges between 0.05% and 0.09%; it was 0.07% at the nominal condition. With the tunnel in the open wall (jet) configuration, the levels are substantially higher, approaching 0.25%.[13]

B. Boundary Layer Trips

The boundary layers on the wing upper and lower surfaces were tripped. A detailed account of the tripping rationale is provided in Ref. 11. To summarize, the size and placement of the boundary layer trips were determined so that fully-turbulent, full-scale flow conditions over the wing surface could be duplicated as closely as possible. Thus, the boundary layer on the lower surface of the wing was tripped from the wing root to the wing tip at a streamwise location corresponding to 9.5% of the local chord. On the upper surface, starting from the wing root, the trip was applied only to the first 67% of span along the wing leading edge. The trip was positioned at 2.5% of the local chord, slightly upstream of the location where peak suction occurs. Tripping the remaining 33% of the wing span proved to be detrimental to the lift and resulted in early stall. Therefore, a decision was made to forgo forced transition and allow the boundary layer to develop naturally for the outer portion of the wing span.

C. Flap 39º (Baseline) Configuration

The steady pressure distributions and global steady aerodynamic characteristics for the baseline configuration are discussed in detail in Ref. 11. Comparison of steady lift and drag forces with the full-scale flight data provided by GAC showed similar lift curve slopes and drag rise with angle of attack, and comparable high Reynolds number stall characteristics. These features indicate that the 18% scale Gulfstream model produces all the relevant trends. For the purposes of this paper, we confine ourselves to the discussion of the fluctuating pressure field in the vicinity of the areas where significant flow unsteadiness exist and thus have the potential to act as prominent airframe noise sources. Note that all the information presented here corresponds to model-scale frequencies.

In Fig. 9, we have plotted the Cp'_{rms} values from all the functioning unsteady probes installed on the model surface. The figure provides a global view of the surface pressure fluctuation levels for various components highlighting the locations where unsteady pressures are relatively high. To demonstrate data repeatability, results from two separate test runs are shown in the figure. Good data repeatability is very important when, as in the present case, the model undergoes numerous configuration changes during the test. In Fig. 9, Run 45 corresponds to the measurements that were obtained during the initial days of the test when no configuration changes had been done to the model yet. Run 108 was a repeat run performed towards the end of the test, after the model had been subjected to a significant number of changes (e.g., flap deflection angles, removal and reinstallation of the main gear, etc.). In general, the majority of the probes (sensors) show excellent data repeatability. Where differences occur, they are mostly confined to the probes on the main landing gear struts. Recalculation of the Cp'_{rms} values, based on the unsteady signals with sub 100 Hz content excluded, revealed that the differences are caused mainly by changes in the low frequency character of the time records. Alterations to the low frequency content of the time signals may have been caused by the numerous instances of main landing gear removal/installation during the test campaign. The necessity to do so forced some of the sensor wiring and static pressure tubes to be lumped inside the gear cavity. The resulting change in landing gear cavity volume would have altered the cavity resonance pressure field and the nature of flow eruption that takes place at the cavity opening.

It is clear from Fig. 9 that the highest pressure fluctuations occur at the flap inboard edge, followed by the flap outboard edge and the main landing gear, the latter two producing comparable levels. The lowest pressure fluctuation levels are found on the gear door, followed by the main body of the flap. Note that there is no repeat data for sensor 66. That sensor was lost toward the middle of the test campaign. Although highly informative, elevated Cp'_{rms} values do not necessarily translate into, or are indicative of, more prominent noise sources. In some instances, the higher Cp'_{rms} values may be produced by the very low frequency content of the measured time signals; as such, they are not very relevant to the airframe noise problem. Better understanding of the fluctuating pressure field is gleaned from observing the processed spectra where the frequency (and the corresponding energy) content of the signals is displayed. PSD data from the unsteady surface probes on different components are given in the following sections. The measurements obtained from probes on the flap main body (probes 18-23) will be discussed in a separate paper, to be presented at a later date.

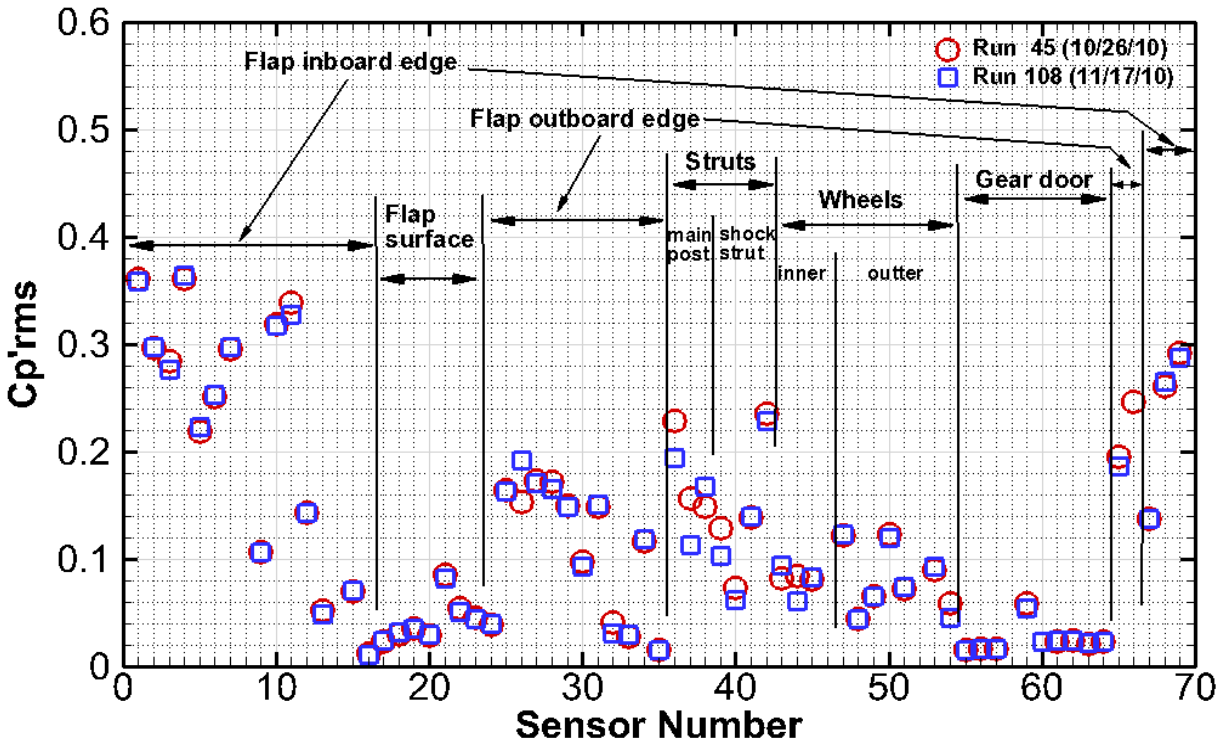

Figure 9. Pressure fluctuation levels from unsteady sensors (probes) installed on 18% model.

1. Flap Inboard Edge

The unsteady pressures at, or in close proximity of, the flap sharp edges play a prominent role in the generation and radiation of high-lift system noise. Acoustic scattering from these edges is important in shaping the local behavior of the noise field and its far field character. Figure 10 shows the surface pressure fluctuation PSD results along the upper surface of the inboard edge. The lowest pressure fluctuations are recorded by probe 67, which is closest to the leading edge. This is surprising, as we had expected the high-amplitude, high-frequency fluctuations to occur in this region where the separated boundary layer is much thinner and the shear layer roll-up/vortex-formation processes take place on shorter spatial scales. The signals from Probes 1 and 5 display a broadband character devoid of any sharp tonal peaks. Probe 1 shows the highest amplitude fluctuations over the widest range of frequencies at the inboard edge. Although probes 2 and 3 also display a broadband character, there seems to be a relatively broad tonal component in the signal between 300 Hz and 1 kHz. The peak of this broadened tone occurs between 520 Hz and 610 Hz.

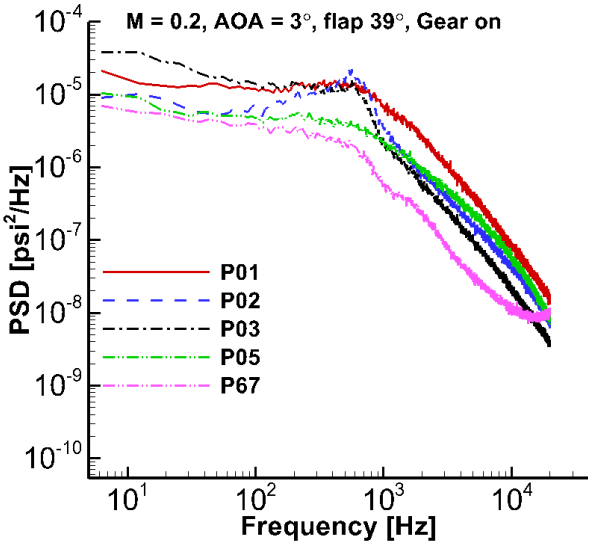

Figure 10. PSD on flap upper surface along inboard edge.

The measured fluctuations from the remaining probes on the inboard upper surface not situated at the edge are shown in Fig. 11. The signal from probe 4 displays a prominent broad peak between 300 Hz and 600 Hz, and is similar in shape to those obtained from probes 2 and 3 (Fig. 10). From the locations of these probes (P02, P03, and P04), it can be seen that the peak is noticeable within a narrow chordwise zone that resides between 60% and 70%

of the flap chord. Based on past experience, the established flow field at a typical flap edge consists of a dual vortex system. We believe that, at this chordwise location, the stronger vortex residing on the side-wall has swung to the top and either has already merged, or is in the process of merging, with the weaker vortex on the upper surface. Notice that the broad peak diminishes rather quickly as the measurement location moves toward the flap trailing edge and away from the side-edge. In fact, at the probe 6 location, which is one flap maximum thickness away from the edge, the footprint of the merged vortices (the broad peak) has disappeared. This reaffirms the notion that the single dominant vortex that results from the merging process scales with the flap-edge maximum thickness. Probe 9, located at the trailing edge, shows a significantly diminished pressure field in the low to mid frequency range. This could be due to the lifting of the vortex path away from the top surface as the trailing edge is approached.

The effect of small variations in the approach angle of attack on flap pressures was also considered. Using probe 2 measurements as an example, note from Fig. 12 that the pressure fluctuations at this location show very little variation with angle of attack. Such invariance was also observed for the steady surface pressures on the flap.[11] This is not surprising, since past experience has shown that the flap pressure field at low to moderate angles of attack depends solely on the flap deflection angle relative to the wing.

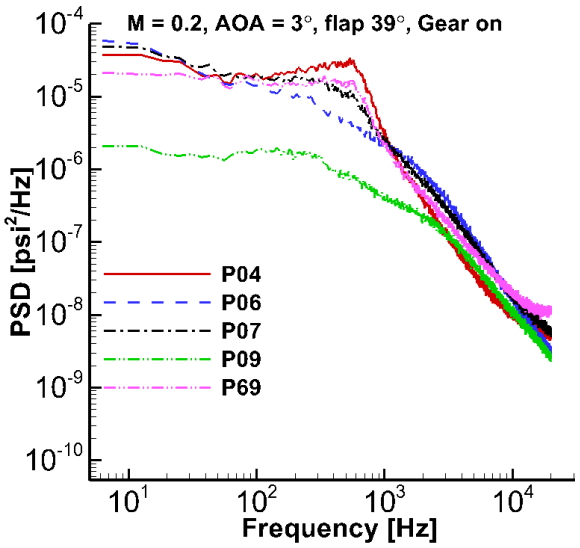

Figure 11. PSD on flap upper surface from probes located away from edge.

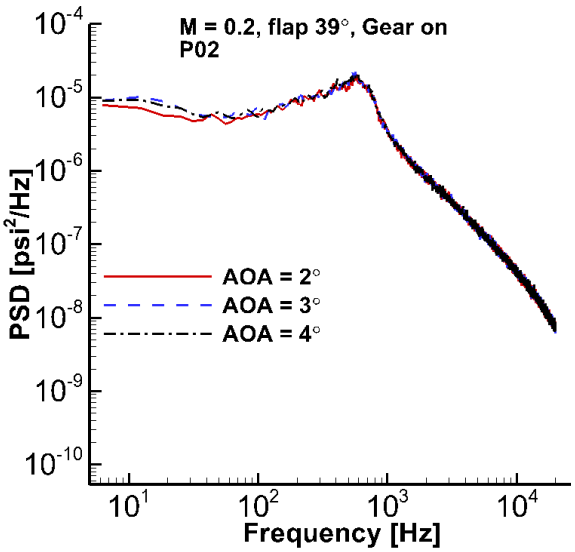

Figure 12. Angle-of-attack effects on probe 2.

The effect of forward speed variations on fluctuating pressure was also examined. Using data from probe 2, Fig. 13 shows that the shape and frequency content of the spectra are similar but shifted in amplitude and peak frequency as the Mach number increases. The measured unsteady pressures show a typical hydrodynamic behavior with the amplitudes scaling with dynamic pressure, Q, and the frequencies with Strouhal number. The three spectra could be collapsed into a single curve (not shown) taking into account these corrections,

The inboard sidewall pressures are explored in Fig. 14. The unsteady pressures collected from probe 11 in the edge mid-chord region have the highest amplitudes at low frequencies, while those associated with probe 68 display the highest levels at high frequencies. Also note that probes 10 and 68, being in close proximity, show similar low-frequency traits. The peak in energy for probe 10 may be related to the early formation stages of the primary vortex on the side wall.

The spectrum from probe 10 (closer to the flap leading edge) is very similar to that obtained from probes 2 and 3 on the upper surface (Fig. 10). As such, it also has a broad tonal peak between 500 Hz and 1,800 Hz. To explore this similarity, the spectra from probes 2, 3, 10, and 11 have been plotted in Fig. 15. Except for a moderate peak frequency shift, it appears that the fluctuating pressures from probes 10 and 2 have similar shape and amplitudes. The same can be said for the spectra obtained from probes 11 and 3. Such a close resemblance suggests a strong interaction between the local flow fields that develop at the edge sidewall and the flap upper surface near the edge. A clearer picture should emerge once the cross correlations between the probes on the side-edge and those on the upper surface are performed.

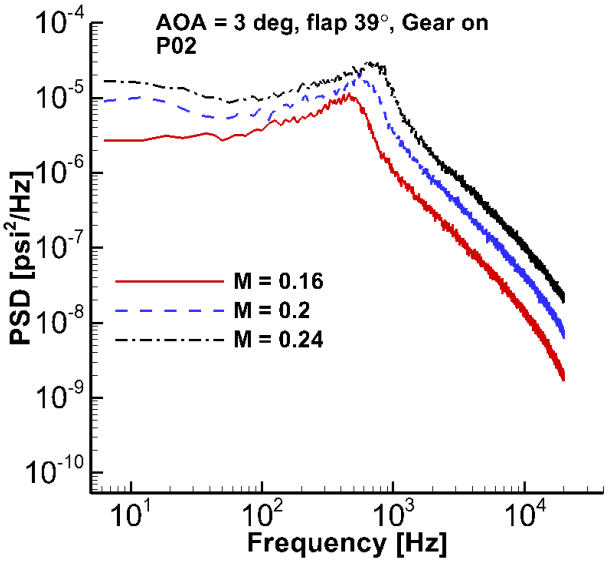

Figure 13. Mach number effects on probe 2.

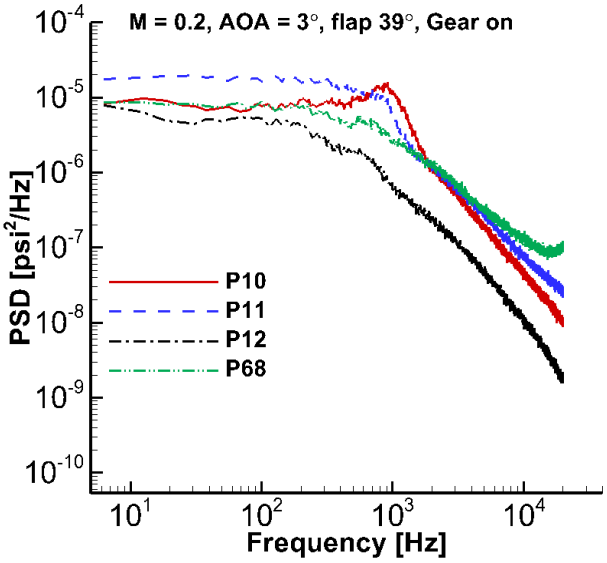

Figure 14. PSD on flap inboard sidewall.

The fluctuating pressure signals recorded from probes on the flap bottom surface at the inboard edge are shown in Fig. 16. As suspected, the two probes positioned at the edge (probes 13 and 15) record higher fluctuation levels. However, even at these elevated levels, the pressure fluctuations are one order of magnitude lower than those recorded on the sidewall and upper surface. The PSD curve from probe 15 shows two very broad peaks, one at low frequencies (centered around 250 Hz) and the second one at moderate frequencies (centered around 1400 Hz). The lowest amplitude pressure fluctuations on the bottom surface are from probe 16, with levels that are more than one order of magnitude smaller than those obtained with probes 13 and 15. Because of the very low pressure levels existing at this location, two narrow tones, one at 230 Hz and another close to 2 kHz, have become visible. The tone at the higher frequency is associated with vortex shedding from the thick trailing edges of the flap and wing adjacent to the inboard edge. The Gulfstream aircraft has unusually thick trailing edges for the purpose of cruise efficiency. We will return to these tones during our discussion of the pressures on the landing gear door.

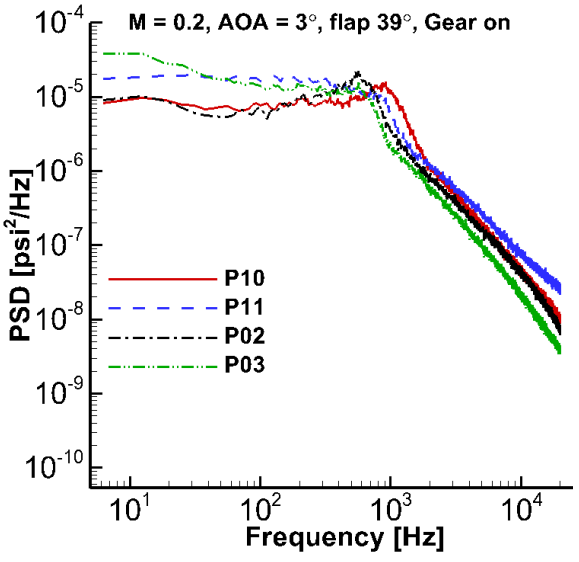

Figure 15. PSD for flap inboard sidewall and upper surface.

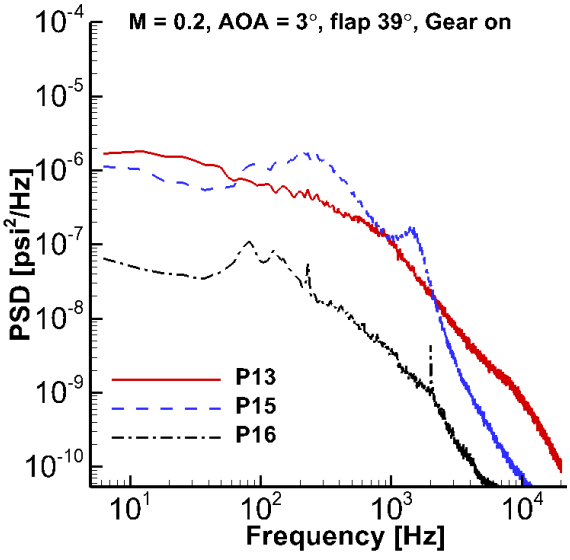

Figure 16. PSD on flap bottom surface at inboard edge.

2. Flap Outboard Edge

The operational aspects of full-scale flaps necessitate the introduction of features such as track rollers, cavities, cut outs of unusual shapes, etc. that are not typical of those studied in model scale experiments. The Gulfstream aircraft is no exception. The outboard flap tip of the aircraft, shown in Fig. 17a, is different from the inboard tip, which has a straight, clean edge. The outboard flap tip has a cavity that runs chordwise, spanning most of the tip length. This cavity houses a bulb seal that acts as a barrier to metal to metal contact during flap deployment/retraction. To maintain high geometric fidelity, the 18% semi-span model flap also possesses a cavity (Fig. 17b) that includes a bulb seal (shown as an orange foam rod). Because of this elaborate tip geometry, we expect the established unsteady flow field at the edge to be complex, resulting in an intricate pressure fluctuation field.

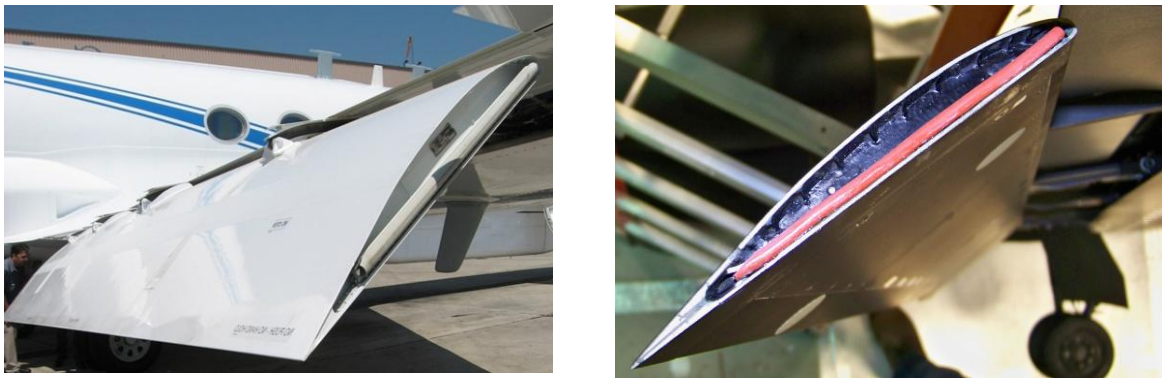

a) Full-scale b) 18% semi-span model

Figure 17. Gulfstream aircraft flap outboard tip geometry.

The fluctuating pressures along the edge on the upper surface are shown in Fig. 18. The probes closest to the flap leading edge (probes 65 and 25), display relatively high levels of energy in the higher frequencies. Moving along the edge towards the flap trailing edge, the high-frequency fluctuations diminish significantly and higher levels appear in the mid and lower range of the frequency spectrum. The pressure fluctuations from probes 65 and 25 have a tonal feature at 6500 Hz. We conjecture that this feature is the result of side-edge vortex-cavity interaction. Conversion of the tone frequency to its full-scale equivalent yields a value that is close to 1200 Hz. Interestingly, phased array and certification microphone measurements from the 2006 flight test[6] also show the presence of a tonal feature at the flap outboard tip with frequency between 1050 Hz and 1400 Hz. However, a more definitive answer on whether these are the same phenomena or a mere coincidence must wait until acoustic measurements of the 18% model, planned for the second phase, become available.

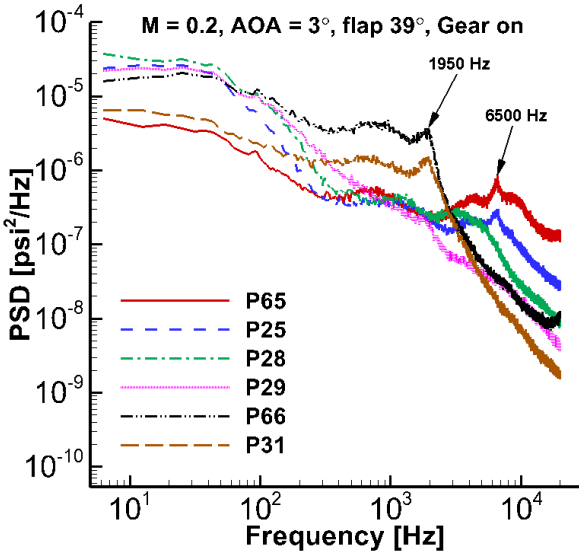

Figure 18. PSD on flap upper surface along outboard edge.

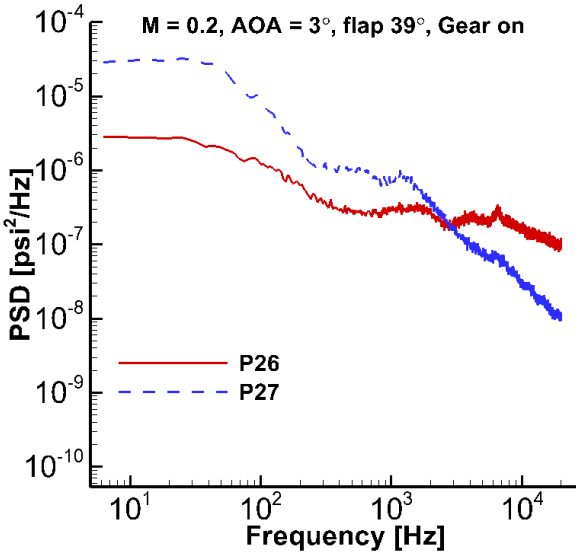

Figure 19. PSD inside outboard tip cavity.

The PSD results from the two transducers installed inside the tip cavity are shown in Fig. 19. The frequency content and the shape of the spectra within the cavity closely track the fluctuating pressures obtained along the edge on the upper surface. That is, the signals from probes 26 and 27 closely resemble those presented for probes 65 and 28, respectively.

The signals from probes 66 and 31 (Fig. 18) suggest the presence of a second tonal feature around 1950 Hz close to the chordwise location where the tip cavity ends. We have also included in Fig. 18 the PSD data from probe 29 to demonstrate that at locations slightly away from the edge, the pressure field character changes drastically, losing much of its mid- and high-frequency content.

Results from all four probes on the bottom surface are plotted in Fig. 20. Except for the probe 34 levels, the fluctuating pressure amplitudes on the bottom surface are orders of magnitude lower than those reported for the upper surface. Notice that the presence of the 6500 Hz tone is clearly captured by the two probes (32 and 33) closest to the flap leading edge. The spectrum shape and fluctuating pressure amplitudes recorded at the probe 34 location are nearly identical to those already shown for probe 31 (Fig. 18), suggesting the presence/passage of common flow features over the two probes.

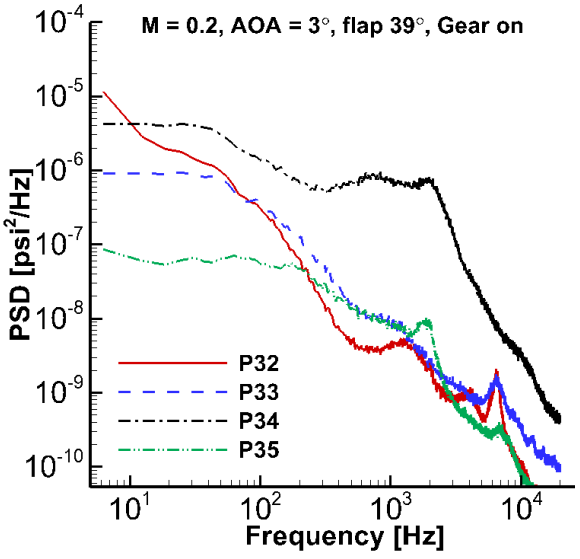

Figure 20. PSD on flap bottom surface at outboard edge.

3. Main Landing Gear

The main landing gear for the 18% semi-span model is a high fidelity replica of the full-scale Gulfstream aircraft geometry including many of the finer structural details (e.g., break system, hydraulic lines, etc.). For the purpose of unsteady pressure measurements, the gear structure was subdivided into its major subcomponents, namely, the two struts, wheels, and door. No pressure measurements from the gear cavity were obtained during the current phase. This shortcoming will be remedied during the second 14x22 entry with the installation of mobile transducers inside the cavity.

a. Main Post and Shock Strut

The pressure fluctuations obtained from the four probes on the shock strut are shown in Fig. 21. The probes were installed in a symmetric pattern around the strut. The two frontal probes (39 and 42) were positioned to capture the wake of the main post. Probes 40 and 41 were placed on the back side of the shock strut to capture the prominent

features of this strut's wake. Note in Fig. 21 that the circumferential fluctuating pressure field is not symmetric due to the presence of the gear door. The signal from probe 39 shows a broad tonal feature centered between 650 Hz and 750 Hz, suggesting that the most probable source of the tone is the main post. The highest amplitude fluctuations are recorded by probe 42, which is on the side of the gear door. The signal from this probe also shows a broad tonal feature centered between 300 Hz and 400 Hz. Given the strut diameter, this frequency is too low to be associated with vortices shed from the shock strut. Probes 40, 41, and 42 show a high level in the fluctuating pressure amplitudes at very low frequencies (below 40 Hz). This level may be associated with massive flow separation on the gear door, or with turbulent flow eruptions from the wheel cavity opening.

The pressure fluctuations recorded by the three probes on the main post are plotted in Fig. 22. The presence of the gear door forces the pressure field in the downstream side of the post to be asymmetric. The signal recorded by probe 37, which is located on the side opposite to the gear door, clearly shows the presence of a tone centered around 650 Hz to 750 Hz. Based on the diameter of the main post and a turbulent shedding assumption, this tone is due to vortex shedding from the post. It is quite likely that the presence of the door suppresses the expected peak in the PSD for probe 38. A comparison of the signals from probes 2 and 3 (located on the upper side of the flap inboard edge) with that from probe 37 suggests that the appearance of a broad tonal feature at the mid-chord region (see Fig. 10) may be associated with the strut-shed vortices impacting the edge. As was the case for the shock strut, the three spectra depicted in Fig. 22 show a significantly higher level of the fluctuation energy at low frequencies, most likely arising from the same sources as those for the shock strut.

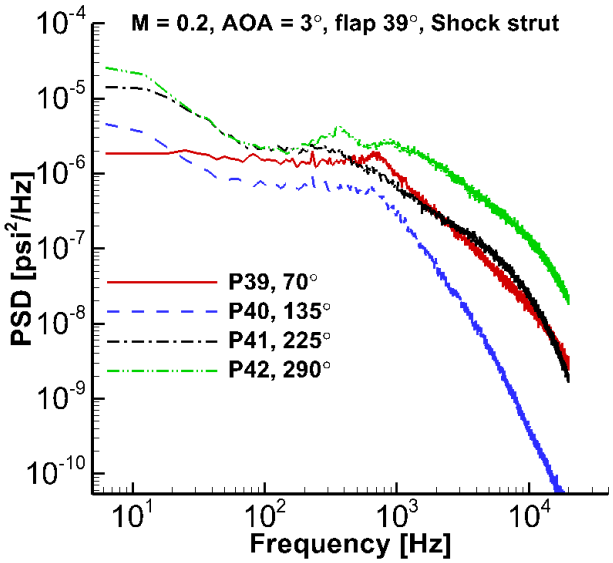

Figure 21. PSD from probes on gear shock strut.

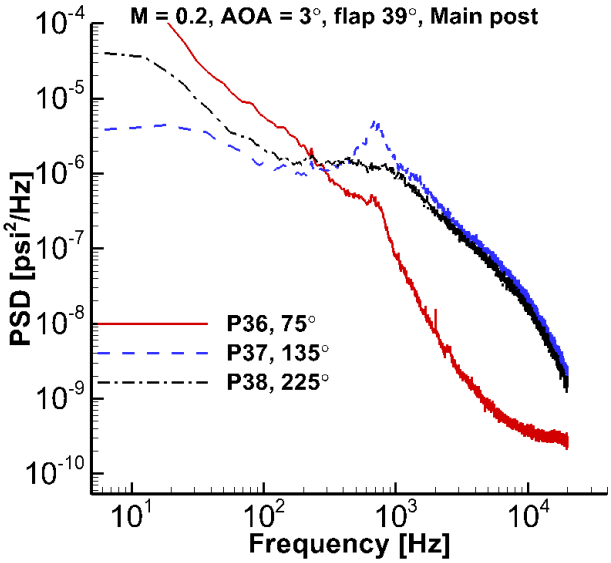

Figure 22. PSD from probes on gear main post.

b. Wheels

The unsteady pressures from the transverse row of probes on the outer wheel are shown in Fig. 23. The probe numbers in the plot legend are ordered in a manner representing the arrangement of the sensors from the hub on the exterior to the ring on the interior of the wheel (see Fig. 6). In general, the lowest fluctuation pressures on the outer wheel over a broad frequency range occur at the tire crown (probe 48) and interior shoulder (probe 54). At the crown location, the fluctuating hydrodynamic pressures are so low (likely due to wheel flow separation) that they allow a 2 kHz tone to be observed. This particular tone is caused by acoustic resonance emanating from a large opening at the knee of the gear's main post. The passage of airflow through the large opening at the knee forces the hollow post to resonate. The same acoustic resonance mechanism was observed during recent testing of an isolated duplicate model of the Gulfstream main landing gear in the Virginia Tech Stability Tunnel (personal communication/unpublished data). In contrast, some of the highest pressure levels appear at a location that is between the crown and outer shoulder of the tire (probe 50). Overall, the higher amplitude pressures occur on the exterior of the wheel. We also note the presence of a second tone at 230 Hz in the probe 51 signal. This tone is associated with wheel cavity resonance, based on the acoustic measurements of the isolated gear model.

Although the lower part of the gear assembly (e.g., tires, brake system, axle, etc.) is symmetric, the door has a noticeable effect on the local flow field surrounding the wheels and the resulting pressure fluctuations. The unsteady

signals from the probes on the inner wheel are shown in Fig. 24. Notice that each inner wheel probe is paired with its counterpart on the outer wheel. Although the PSD data from locations on the interior side-wall of the tires (probes 44 and 49) are similar, the fact that none of the pairs produce identical PSD curves is a clear indication that the pressures on the two wheels are different: note that, for frequencies higher than about 400 Hz, the location on the outer wheel where the highest pressure fluctuation levels were observed (probe 50) produces the lowest pressure fluctuation levels on the inner wheel (probe 45). This may be caused by higher flow velocities in the vicinity of the outer wheel shoulder (where probe 50 is located) induced by the presence of the door. The associated higher velocity gradients could enhance the high-speed fluctuation levels. Conversely, if the flow velocity on the shoulder of the inner wheel (where probe 45 is located) is lower, the fluctuation levels may be suppressed due to lower velocity gradients.

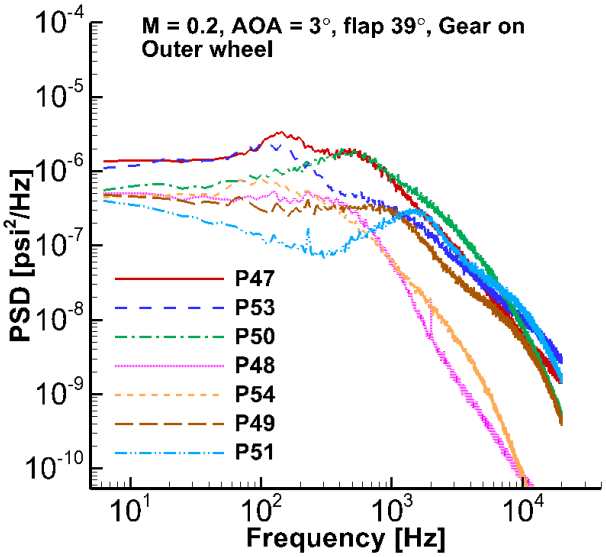

Figure 23. PSD along a transverse row on outer wheel.

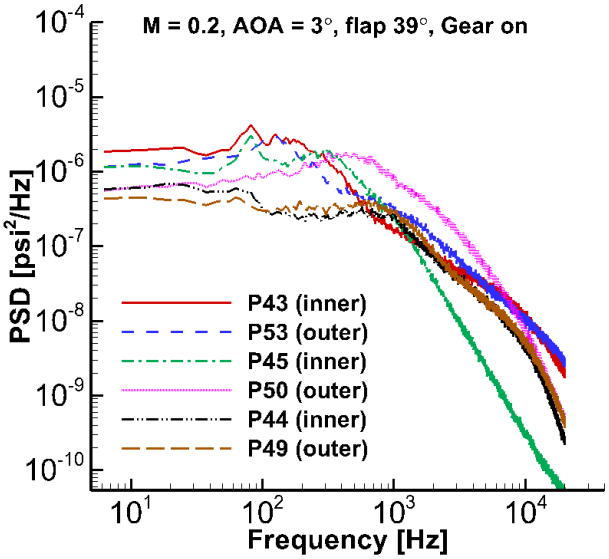

Figure 24. Inner and outer wheels PSD.

c. Door

Recall from Fig. 9 that the weakest pressure fluctuations are produced on the door. Depending on the incoming flow angle relative to its leading edge, the door surface most likely encounters a massively separated flow. As such, the low speed air adjacent to the surface produces low amplitude pressure fluctuations. However, because of its shape and slanted orientation, the door acts as a good acoustic reflector.

The PSD data from four of the door probes are plotted in Fig. 25. The selected data illustrate nicely the development of the fluctuating pressure field along the door width. Commensurate with the door Cp'_{rms} values, the spectra clearly show that the fluctuating pressures are orders of magnitude lower over the entire frequency range than at most other locations on the model. Notice that the PSD curves from all four probes are similar in shape and magnitude, showing a continuous drop in the broadband pressure levels with increasing frequency. Because of the extremely low pressure levels, three tones emerge as prominent features in these spectra. As described earlier, the 230 Hz and 2 kHz tones are due to the acoustic resonances from the wheel cavity and main-post-knee opening, respectively. Although not shown, the resonant nature of these two tones was confirmed by comparing the spectra at the three measured speeds. The tonal frequencies did not shift in a manner that was commensurate with the speed variation. In

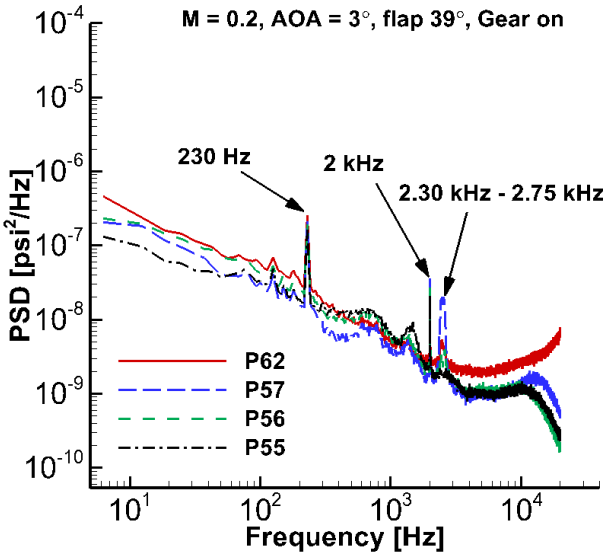

Figure 25. Pressure fluctuations on gear door.

contrast, the third tone, centered between 2.3 kHz and 2.75 kHz, showed a hydrodynamic behavior with the proper shift in frequency and amplitude that is typical of bluff body vortex shedding. The flap and wing in the vicinity of the inboard edge possess trailing edges that are approximately 0.215 in (0.0055 m) thick. Assuming a turbulent Strouhal shedding of 0.22 from the trailing edge, the M = 0.2 speed produces a shedding frequency on the order of 2.7 kHz which is within the band highlighted in Fig. 25. The acoustic waves radiating from these three sources (tones) impinge upon the door and are partially reflected towards an observer on the ground.

D. Gear-Flap Interaction Effects

A poorly understood airframe noise source is gear–flap interaction noise. For many aircraft, the spanwise position of the main landing gear after deployment is almost coincident with the flap inboard edge. The wake shed by the main gear interacts directly with the flap inboard edge, and has the potential to generate high-amplitude pressure fluctuations and thus noise. In Ref. 11, a comparison of lift coefficient (C_L) as a function of angle of attack with the main gear on and off showed negligible differences. This indicates that gear removal (retraction) has little influence on the global lift distribution. No such claim can be made with regard to local effects, and these drive the generation of airframe noise.

To examine how the wake from the main gear affects the inboard edge flow field, we first begin with the time-averaged pressure field. Fig. 26, taken from Ref. 11, shows pressure coefficient (Cp) distributions for the first two rows near the inboard edge. The first row of pressure orifices is located very close to the side-edge; the second row is situated farther from the edge at a spanwise distance corresponding to 1.6 times the local flap edge maximum thickness. Note that removal of the gear has a profound effect on the loading at the inboard edge and results in higher lift for the configuration without the gear. Based on these pressure differences, the absence of the gear wake enhances vortex roll-up at the edge and produces stronger vortices. As a result, one may surmise that the associated unsteady surface pressure field would also show significant differences. As will be discussed below, this indeed is the case.

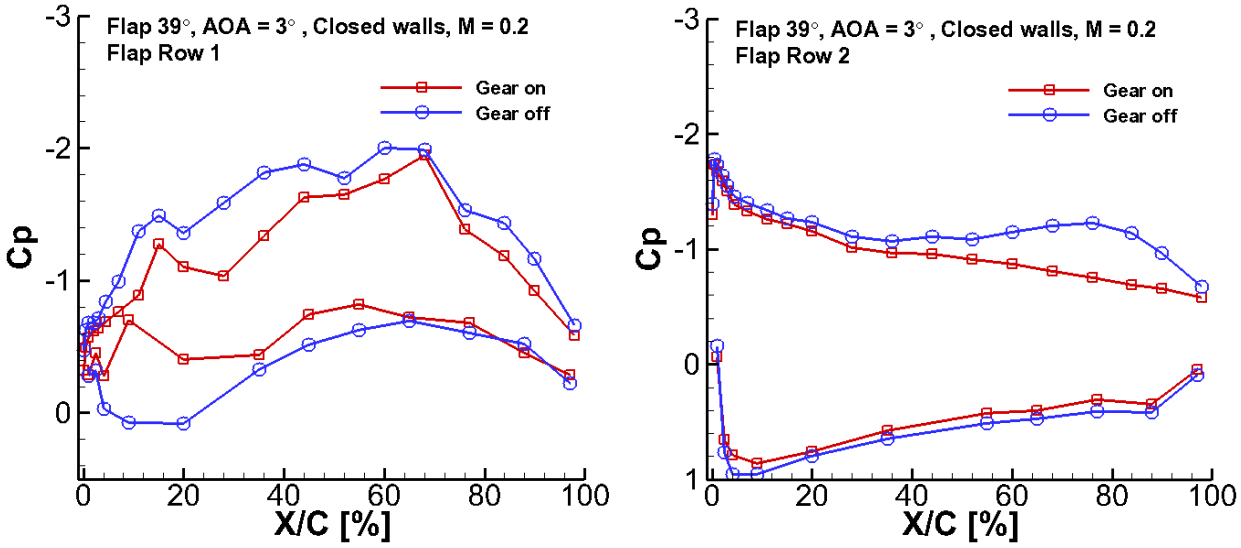

a) First row from the edge. b) Second row from the edge.

Figure 26. Effect of main gear removal on the steady pressure distribution near the inboard edge.

With the exception of probe 10, removing the gear generally lowers the pressure fluctuation amplitudes at those probe locations that are on the inboard edge sidewall or on the flap upper surface adjacent to the edge. The largest decrements occur in the flap mid-chord region. Pressure fluctuations at probes 1 and 2, located on the flap inboard upper edge, with gear on and off are shown in Fig. 27. Note that absence of the gear has a profound effect on the fluctuations and results in an order of magnitude drop in their amplitude over a large range of frequencies. Also gone is the broad tonal feature in the probe 2 spectrum that was centered around 575 Hz. The absence of this feature lends support to the conjecture that strong unsteady flow structures in the gear wake impinge on the flap inboard edge. The corresponding plots for probes 3 and 5, which are located further downstream in the mid-chord region, are shown in Fig. 28. As indicated earlier, the magnitude of the drop in fluctuation amplitude is reduced at these locations with the change mostly confined to frequencies below 3 kHz.

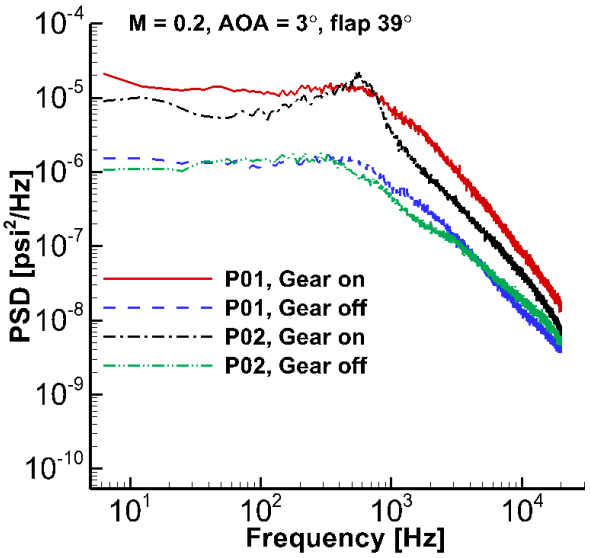

Figure 27. Gear effects on probe 1 and 2 PSD.

On the inboard edge sidewall, the effect of gear removal on the pressure fluctuations is most drastic at the probe 11 location as shown in Fig. 29. Although a drop in fluctuating pressure amplitude is observed over the entire measured frequency range, the most significant change is confined to frequencies below 1 kHz. Given the position of the landing gear relative to the 39º flap inboard edge, the wakes emanating from the two gear struts are surmised to be the prime contributors to the drop in fluctuating pressure between 50 Hz and 1 kHz.

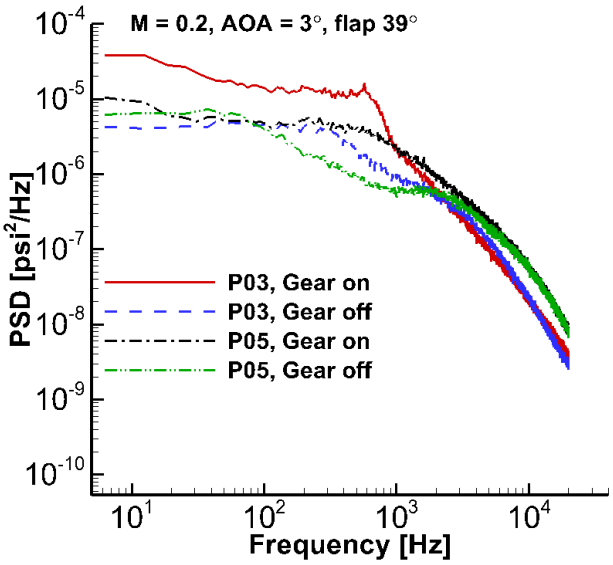

Figure 28. Gear effects on probe 3 and 5 PSD.

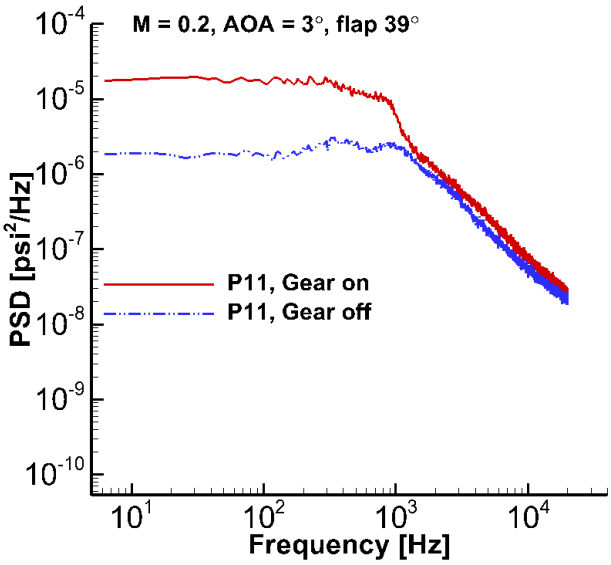

Figure 29. Gear effects on probe 11 PSD.

F. Closed vs. Open Walls Tunnel Configuration

The planned acoustic and off-surface (particle image velocimetry) flow measurements require that the tunnel be in an open-wall (open-jet) configuration. In this mode, the reverberating effects of the tunnel walls on the acoustic field are eliminated and better optical access for the flow measurements is gained. Associated with open-wall testing, however, is the possibility of introducing other factors that may negatively impact the aerodynamic characteristics of the model. While the model scale was selected based on conservative estimates, there was no a priori guarantee that the efficiency of the 14x22 tunnel could be maintained with side walls and ceiling removed. Depending on the model size and how much lift it produces, the open jet may be deflected substantially and severely

affect the performance of the model. In particular, for the present case where the high-lift aerodynamic performance through stall is desired, the impact of testing in open-wall tunnel configuration had to be carefully documented. Comparison of the steady aerodynamic measurements obtained with the tunnel in the closed- and open-wall configurations, as reported by Khorrami et al.,[11] showed that the aerodynamic behavior of the model is consistent over the entire angle of attack range, including the stall regime. Here, we present the effects of tunnel configuration on the model unsteady pressure field.

For the critical case of the model in landing configuration, we have carefully compared the measured unsteady pressures from every probe with the tunnel in the closed- and open-wall configurations. Except for two probe locations on the main gear, the recorded pressures from the two tunnel configurations are virtually indistinguishable. To illustrate this near perfect agreement, representative plots from the flap inboard edge (probe 01) and from the outboard edge (probe 25) regions are shown in Fig. 30. Fluctuating pressures for the two probe locations (probes 38 and 59) where some differences were observed are shown in Fig. 31. These probes are located close to each other – probe 38 resides on the door side of the gear's main post and probe 59 on the door surface. Note from the figure that the only effect associated with open tunnel walls is a uniform, moderate drop in the pressure amplitudes across the entire frequency range. However, the spectrum shape and frequency content at the two affected probe locations remain unchanged.

A preliminary analysis of the correlation between the accelerometers and the unsteady pressure sensors on the flap shows evidence of flow induced vibrations. The vibrational effects are manifested in the PSD results and often become apparent when the overall PSD levels are very low. This relationship will be examined at a later time.

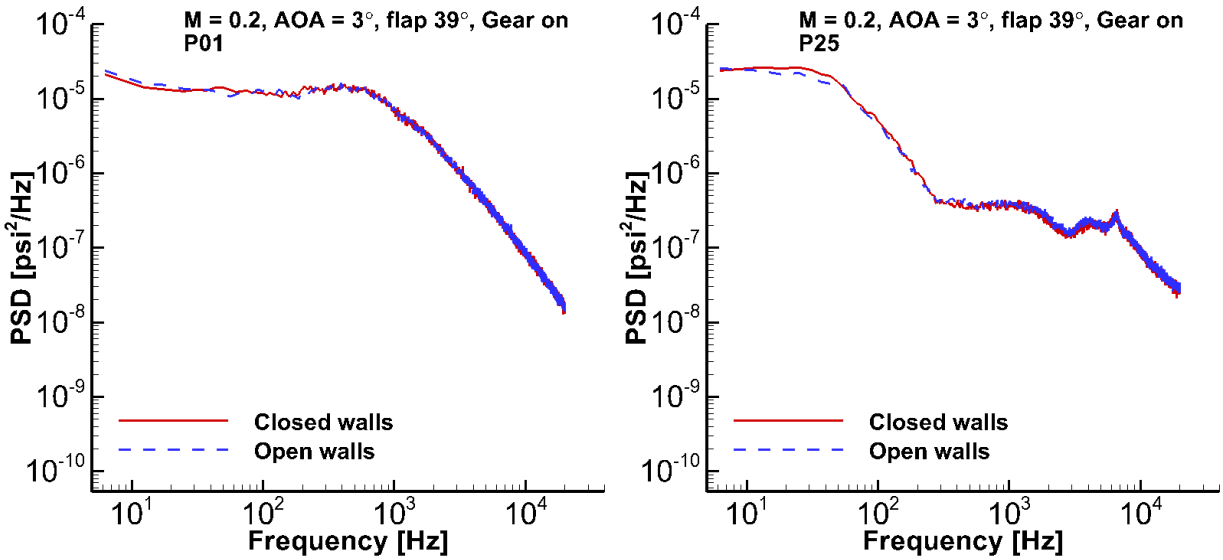

a) inboard edge b) outboard edge

Figure 30. Tunnel configuration effects on surface pressure fluctuations.

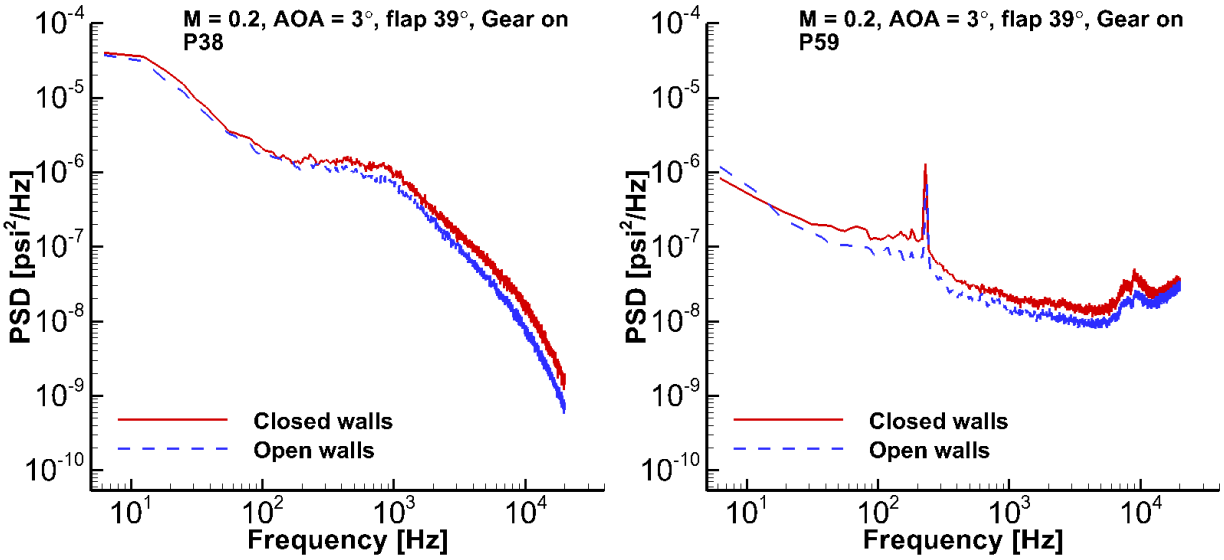

a) gear main post b) gear door

Figure 31. Comparison of PSD from the two affected probes by the change in tunnel configuration.

G. Coherence Results

Valuable insight on the structural character of the fluctuating pressure field is gained from an analysis of the coherence and cross-correlation data by pairing signals from individual probes to discern similarities/interactions between them. Due to the vast amount of data collected during the experiment, the full analysis will be presented at a later date. In this paper, we limit ourselves to a preliminary subset of recently computed coherence results, with focus on the gear struts and gear-flap flow interaction. As will be seen in Figs. 32 through 36, coherence data for various sensor combinations showed significantly higher levels at very low frequencies (below 100 Hz). There are two main sources of flow unsteadiness that cause high coherence levels at low frequencies. One source is associated with the large region of flow separation that occurs on the flap main body; the other source is related to the fluctuating flow field at the gear-cavity opening. Due to their very low frequencies, these two sources are not relevant to airframe noise phenomena.

The coherence values between probes on the main post, and probes on both main post and shock strut, are presented in Fig. 32. The results indicate that high coherence exists among the probes that are located on the side opposite to the gear door. This high coherence occurs in a relatively narrow frequency band centered around 685 Hz. As indicated earlier during the discussions of the PSD data, this frequency corresponds to turbulent bluff body shedding from the main post. In Fig. 32, we have also included coherence values between probes that are located on the door side (probes 38 and 42). As we have alluded to previously, this lack of coherence highlights the effect of the door in suppressing the vortex shedding process on that side.

The peak in PSD plots observed for probes 2, 3, and 37 (Figs. 10 and 22) led us to postulate the possibility that vortices shed from the gear struts are convected downstream and ultimately impinge upon the flap inboard edge. To examine the validity of such a scenario, we have computed the coherence values between any possible paring of the probes on the gear struts and the probes at the flap inboard edge. Surprisingly, except at very low frequencies, near zero coherence values are observed from such pairs. Representative coherence plots between probes on the gear struts and probe 3 at the inboard edge are shown in Fig. 33. The near zero coherence suggests that by the time the gear wake arrives at the side edge, it is devoid of any coherent large scale structures. Also shown in Fig. 33 are the coherence values between probe 36 on the main post and probe 16 on the bottom surface near the trailing edge of the flap. This particular pairing produced the only non-negligible coherence values, namely, the two resonance tones originating from the gear.

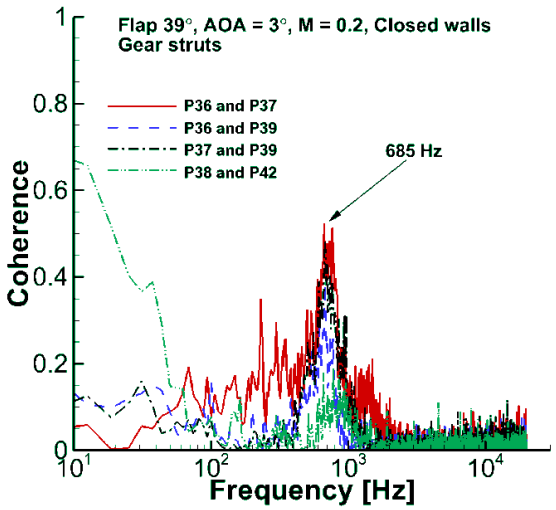

Figure 32. Coherence data for main post, and post and shock strut.

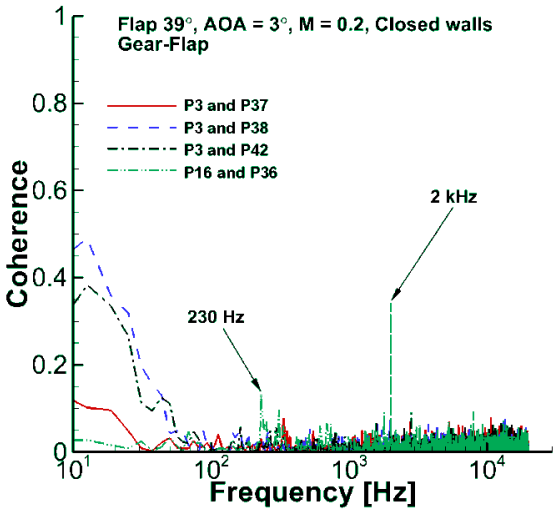

Figure 33. Representative coherence values between gear struts and flap inboard edge.

The highest coherence values at the flap inboard edge are obtained between probes that are positioned within the 60% to 80% chordwise distance from the flap leading edge. This is the region where the vortex on the side wall outgrows the edge thickness, spills over the top, and begins to merge with the vortex located at the edge on the upper surface. Representative plots showing the coherence between probe 2 and several other probes in the vicinity are shown in Fig. 34. All plotted curves show that peak coherence levels occur at 575 Hz. We believe that this frequency is associated with the edge vortices. Also notice near zero correlation at frequencies greater than 2 kHz, indicating that the coherent structures (the dual vortex system) at the flap inboard edge are a fairly low frequency event. In Fig. 34 near perfect coherence is observed at 575 Hz between probes 2 and 4, rather than between probes 2 and 3. It is noted that probe 3, located at the edge, is at the same chordwise location as probe 4. Therefore, a good correlation between probes 2 and 4 suggests that, once on the upper surface, the primary vortex takes a path slightly inward of the edge rather than remain at the edge.

Sample coherence plots for the probes near the flap leading edge at the outboard edge are shown in Fig. 35. The selected probes relate the pressure signals on the top surface (probes 24 and 25) and within the tip cavity (probe 26) to the fluctuations recorded at the edge on the bottom surface (probe 32). The coherence plots clearly illustrate that the character of the fluctuations at the outboard edge is very different than that at the inboard edge (see Fig. 34). An important distinguishing feature is the presence of relatively high coherence levels at higher frequencies than those observed at the inboard edge. Also note from Fig. 35 that the coherence curve associated with each probe pair possesses multiple peaks that are quite distinct. The 6.5 kHz tonal feature, attributed to the vortex-cavity interaction, is very prominent in these plots. We believe that the high coherence levels observed for frequencies below 300 Hz are induced by the massively separated flow on the top surface of the flap near the outboard tip.

Using the coherence levels between probes 6 and 7 at the inboard edge as an example, the tunnel configuration and gear removal effects are shown in Fig. 36. Probes 6 and 7 were selected for this purpose because the correlation between the two provides a good indication of the inward movement of the post merger vortex. As expected, the coherence data of Fig. 36 reinforce the observations made from the PSD plots of Fig. 30, showing near identical values for both tunnel configurations when the gear is on. Removing the gear significantly alters the coherence values, nearly doubling the peak magnitude and spreading the coherence function to lower frequencies. We have just begun to examine the interrelationship between the recorded signals from various pairs of probes for different model/tunnel configurations. Therefore, discussion of the full set of coherence and cross-correlation data will be presented in a future paper.

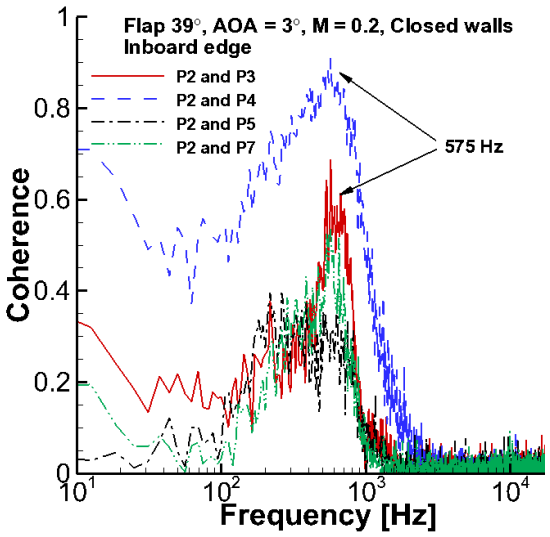

Figure 34. Coherence data from probes at flap inboard edge.

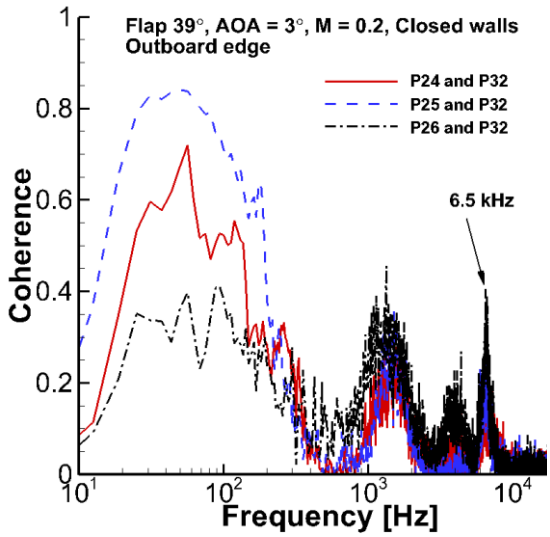

Figure 35. Coherence data from probes at flap outboard edge.

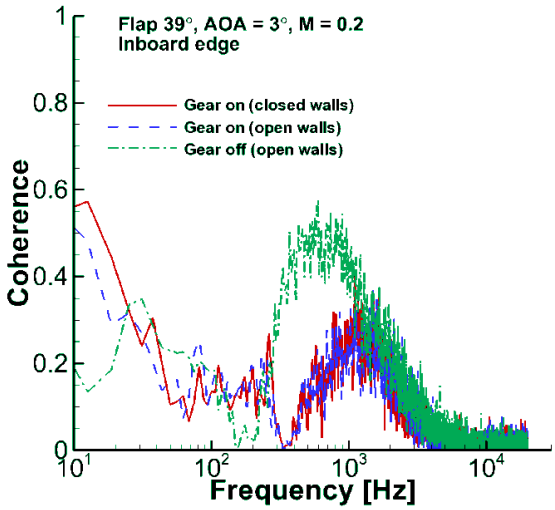

Figure 36. Coherence data showing effects of tunnel configuration and gear removal, P6 and P7.

IV. Concluding Remarks

Under an ongoing NASA-Gulfstream partnership, an 18% scale semi-span model of a Gulfstream aircraft was designed and fabricated to conduct airframe noise research and develop effective noise reduction technologies. A high level of geometric fidelity was maintained for the model to allow direct comparison with the previously obtained full-scale acoustic data and with results from upcoming flight tests. The model was instrumented with a significant number of surface mounted static ports and dynamic sensors to capture the overall character (global and local) of the steady and unsteady pressure fields. Testing of the 18% model is to be accomplished in two phases. The initial phase, reported here, was conducted in the LaRC 14x22 tunnel to fully map the aerodynamic characteristics of the model. Flap deflection angles of 39º, 20º, and 0º with the main landing gear on and off were tested at Mach numbers of 0.16, 0.20, and 0.24. Only results for the 39º flap deflection (landing condition) are presented in this paper. Additionally, for each configuration, the model was tested with the 14x22 tunnel both in the closed-wall and open-wall (jet) modes. During this entry, measurements of the global forces (lift and drag) plus extensive steady and unsteady surface pressures were acquired. The former are presented in a companion paper.

Fluctuating pressures were generally found to repeat very well during the entire test, which involved numerous model configuration changes. Observation of the unsteady RMS pressure coefficient, Cp'_{rms}, from the surface mounted probes revealed that the highest pressure fluctuation levels occured at the flap inboard edge followed by the outboard edge and main landing gear struts. Power spectral density (PSD) results were used to discern some of the intricate features of the unsteady pressure field at critical locations where prominent airframe noise sources are located. The PSD data at the flap inboard edge revealed the fluctuating pressure field to be dominated by relatively low frequency events. At this edge, the recorded signals at most probe locations near the mid-chord region showed the presence of a very broad tonal feature centered around 575 Hz. This feature is attributed to the primary vortex on the side wall and its interaction, and eventual merger, with the weaker vortex on the top surface. The pressure field at the flap outboard edge demonstrated a highly complex behavior due to the presence of a cavity at the tip. The PSD data revealed significant fluctuation activity at higher frequencies than those observed at the inboard edge. The appearance of a 6.5 kHz tonal feature in the PSD data from probes near the flap leading edge is attributed to vortex-cavity interaction. The recorded signals from the gear struts captured the presence of vortices being shed from the main post. Vortex shedding was found to occur on one side only, being suppressed on the side where the gear door is located.

As was the case for the steady pressures reported in Ref. 11, moderate changes in the angle of attack had negligible effects on the fluctuating surface pressures. Similarly, Mach number variation showed no significant effects, other than the expected hydrodynamic behavior of the surface pressures (i.e., the pressure amplitudes scaled with the dynamic pressure and the frequencies scaled with the Strouhal number).

Interaction of gear-wake with the flap inboard edge was studied in detail. To the best of our knowledge, this critical flow interaction had not been investigated previously using a realistic aircraft configuration. Removal of the gear was shown to have a profound effect on both the steady and unsteady surface pressures at the inboard edge. With the gear removed, the fluctuating pressure field showed an order of magnitude increase in PSD levels for most of the sensor locations.

Limited coherence data from select sensors was presented for the cases of strut-to-strut, strut-flap inboard edge, and between sensors on the inboard edge or outboard edge. Coherence between sensors on the two struts showed the expected high levels within a narrow frequency range, indicative of the vortex shedding process. However, as observed in the PSD results, coherence suppression on the side of the strut where the door was placed also existed, giving weight to the significant effect of the door's presence. The calculated coherence revealed no direct correlation between the recorded pressures on the gear struts and those on the flap inboard edge, indicating that by the time the gear wake arrives at the side edge, it is devoid of any coherent large scale structures. Coherence data for sensors on the flap inboard edge showed significantly high levels at low frequencies, most likely associated with edge vortex dynamics. The coherence results from the flap outboard edge revealed significant activity at high frequencies capturing a tonal component attributed to vortex-cavity interaction.

Tunnel configuration changes (closed-wall vs. open-wall mode) had no significant effects on the unsteady surface pressure fluctuations. Together with the steady aerodynamic results presented in Ref. 11, this favorable comparison alleviates most of the concerns and trepidations associated with open-jet testing. As a result, the acoustic and off-surface flow measurements, planned for the second entry, will be conducted with the 14x22 tunnel in the open-wall mode. It is anticipated that the present aerodynamic data, together with the second phase off-surface velocity and far field acoustic measurements, augmented with full-scale data, will constitute a comprehensive and unique dataset to validate and improve our prediction tools for airframe noise.

Acknowledgments

This work was supported by the Environmentally Responsible Aviation (ERA) project under the Integrated System Research Program (ISRP) of NASA. As is the case with the development of any large scale model, the design, fabrication, and instrumentation of the present 18% scale model were the culmination of many years of hard work by a dedicated group of people (too numerous to be listed here) at the NASA Langley Research Center. Some of the key personnel leading the model development task were William D. Castle, Scott Verden, Glenn Ormsby, Robert Harris, Gary Wainwright, and Sandy Webb. Special thanks go to E. Thomas Hall for masterfully instrumenting the model far beyond what was deemed possible. We also would like to thank the staff of the Langley 14x22 facility for their outstanding support and execution of a highly productive test entry. We appreciate the support provided by Donald Day during model installation in the 14x22 tunnel. In addition, we would like to express our gratitude to Luther Jenkins and Meelan Choudhari for their valuable assistance in resolving the boundary layer transition issues and the placement of the boundary layer trips at the leading edge of the wing.

We would also like to acknowledge the contributions of the GAC Applied Aerodynamics and Acoustics Groups, and other Gulfstream personnel, for their many services enabling the design and testing of the 18% scale Semi-span model. In particular, the invaluable support from Thomas Van de Ven of the Acoustics Group is greatly appreciated.

References

[1]Michel, U., Barsikow, B., Helbig, J., Hellmig, M., and Schüttpelz, M., "Flyover Noise Measurements on Landing Aircraft with a Microphone Array," AIAA Paper 98-2336, May 1998.

[2]Piet, J.-F., Elias, G., and Lebigot, P., "Localization of Acoustic Sources from a Landing Aircraft with a Microphone Array," AIAA Paper 99-1811, May 1999.

[3]Pott-Pollenske, M., Dobrzynski, W., Buchholz, H., Gehlhar, B., and Walle, F., "Validation of a Semiempirical Airframe Noise Prediction Method through Dedicated A319 Flyover Noise Measurements," AIAA Paper 2002-2470, June 2002.

[4]Stoker, R., Guo, Y., Streett, C. L., and Burnside, N., "Airframe Noise Source Locations of a 777 Aircraft in Flight and Comparisons with Past Model Tests," AIAA Paper 2003-3232, May 2003.

[5]Elkoby, R., Brusniak, L., Stoker, R., Khorrami, M. R., Abeysinghe, A., and Moe, J. W., "Airframe Noise Results from the QTD II Flight Test Program," AIAA Paper 2007-3457, May 2007.

[6]Khorrami, M. R., Lockard, D. P., Humphreys, Jr., W. M., Choudhari, M. M., and Van de Ven, T., "Preliminary Analysis of Acoustic Measurements from the NASA-Gulfstream Airframe Noise Flight Test," AIAA Paper 2008-2814, May 2008.

[7]Horne, W. C., James, K. D., Arledge, T. K., Soderman, P. T., Burnside, N., and Jaeger, S. M., "Measurements of 26%-scale 777 Airframe Noise in the NASA Ames 40- by 80 Foot Wind Tunnel," AIAA Paper 2005-2810, May 2005.

[8]Jaeger, S. M., Burnside, N. J., Soderman, P. T., Horne, W. C., and James, K. D., "Microphone Array Assessment of an Isolated, 26%-Scale, High Fidelity Landing Gear," AIAA Paper 2002-2410, June 2002.

[9]Neuhart, D. H., Khorrami, M. R., and Choudhari, M. M., "Aerodynamics of a Gulfstream G550 Nose Landing Gear Model," AIAA Paper 2009-3152, May 2009.

[10]Zawodny, N. S., Liu, F., Yardibi, T., Cattafesta, Jr., L. N., Khorrami, M. R., Neuhart, D. H., and Van de Ven, T., "A Comparative Aeroacoustic Study of a ¼-Scale Gulfstream G550 Aircraft Nose Landing Gear Model," AIAA Paper 2009-3153, May 2009.

[11]Khorrami, M. R., Hannon, J. A., Neuhart, D. H., Markowski, G. A., and Van de Ven, T., "Aeroacoustic Studies of a High-Fidelity Aircraft Model: Part 1—Steady Aerodynamic Measurements," Paper to be presented at the AIAA/CEAS Aeroacoustics Conference, June 2012.

[12]Bendat, J. S. and Piersol, A. G., *Randon Data: Analysis and Measurement Procedures*, John Wiley & Sons, New York, 2000, Chap. 8.

[13]Gentry, C. L., Jr., Quinto, P. F., Gatlin, G. M., and Applin, Z. T., "The Langley 14- by 22-Foot Subsonic Tunnel: Description, Flow Characteristics, and Guide for Users," NASA TP-3008, 1990.

[14]Neuhart, D. H. and McGinley, C. B., "Free-Stream Turbulence Intensity in the Langley 14- by 22-Foot Subsonic Tunnel," NASA TP-2004-213247, 2004.